

Graphene Transistors and Photodetectors

by Alexander V. Klekachev, Amirhasan Nourbakhsh, Inge Asselberghs, Andre L. Stesmans, Marc M. Heyns, and Stefan De Gendt

Graphene is an atomically thin crystalline film formed by sp^2 -hybridized carbon atoms. It has a unique electronic structure substantially different from that of materials traditionally employed in solid-state electronics. Graphene is a semimetal with a zero band overlap (or semiconductor with zero band gap), linear energy dispersion, and linear density of electronic states.¹ In the low energy range with respect to the Fermi level, the conduction and valence bands form conic shapes (referred as “Dirac cones”) and meet each other at the so called Dirac points.² One of the most important properties of graphene is a strong electric field effect which leads to an electrostatically tunable carrier density in the range of $n < 10^{14} \text{ cm}^{-2}$. Together with high carrier mobilities for both electrons and holes³⁻⁴ (as high as $10^4 \text{ cm}^2/\text{Vs}$ at room temperature), this attracts a lot of attention to graphene as a possible material for a future high-speed field effect transistor (FET).⁵

The two-dimensional nature of graphene is another fact responsible for the rapid growth of its research, leaving behind other sp^2 -carbon allotropes.⁶ Micromechanical cleavage of graphite can lead to the formation of single atom thick continuous graphitic films over Si/SiO_2 surfaces.⁷⁻⁸ Graphene

allows simple optical identification methods at the particular thickness of SiO_2 , Al_2O_3 , or other dielectric layers on Si .⁹ It requires only conventional planar processing technologies available within existing rich CMOS expertise.

The most often studied graphene FET structure is a back-gated configuration (Fig. 1a) where the graphene flake is contacted to form source and drain electrodes and the substrate acts as a back gate. By depositing a dielectric layer on top of such device, one can achieve a top-gate configuration (Fig. 1b) allowing both gate biases to control the charge concentration in the device channel.⁴ Alternatively, by synthesizing graphene on silicon carbide wafers (SiC)¹⁰ covering the whole SiC wafer, a large number of devices each having only one (top) gate can be fabricated (Fig. 1c).¹¹⁻¹² Figure 1d shows a typical transfer curve for the graphene FET. The maximum channel resistance (or minimum conductance) corresponds to the position of the Fermi level at the Dirac point and is located at $V_G = V_{\text{NP}} \sim 9\text{V}$ (NP-neutrality point) for the sample shown in Fig. 1d, due to minor p-doping of graphene. Various examples of adsorbed species, ranging from metals and adatoms,¹³ to organic compounds,¹⁴ inorganic salts,¹⁵ and gases¹⁶ can provide either n- or p-type

doping in graphene. The part of $\rho(V_G) < V_{\text{NP}}$ corresponds to hole conductance while $\rho(V_G) > V_{\text{NP}}$ corresponds to electron conductance as indicated schematically with the Dirac cones in Fig. 1d.

Due to its semimetallic nature, the graphene FET channel has a low resistance modulation ratio $\rho_{\text{ON}}/\rho_{\text{OFF}} \sim 6$. This ratio, often referred as current ratio $I_{\text{ON}}/I_{\text{OFF}}$, does not exceed 10 at room temperature, therefore, the use of graphene for logic devices, where the minimum required $I_{\text{ON}}/I_{\text{OFF}}$ exceeds 10^3 , is unfavorable.¹⁷ Nevertheless, graphene was found to be attractive for high-speed analog electronics, where transistor current gain is more important than $I_{\text{ON}}/I_{\text{OFF}}$.¹⁸ Transistors having cut-off frequencies as high as 350 GHz and high frequency circuits were recently demonstrated.¹⁹⁻²⁰

One way to overcome the zero-band gap problem is to induce lateral quantum confinement, *i.e.*, by shaping the graphene into graphene nanoribbons (GNR) in the sub 10 nm regime. This may improve the $I_{\text{ON}}/I_{\text{OFF}}$ ratio of the transistor. In GNR two distinct types can be considered depending on the configuration of the C-atoms at the edges of the ribbon. Both armchair and zig-zag structures can be obtained, and the energy

(continued on next page)

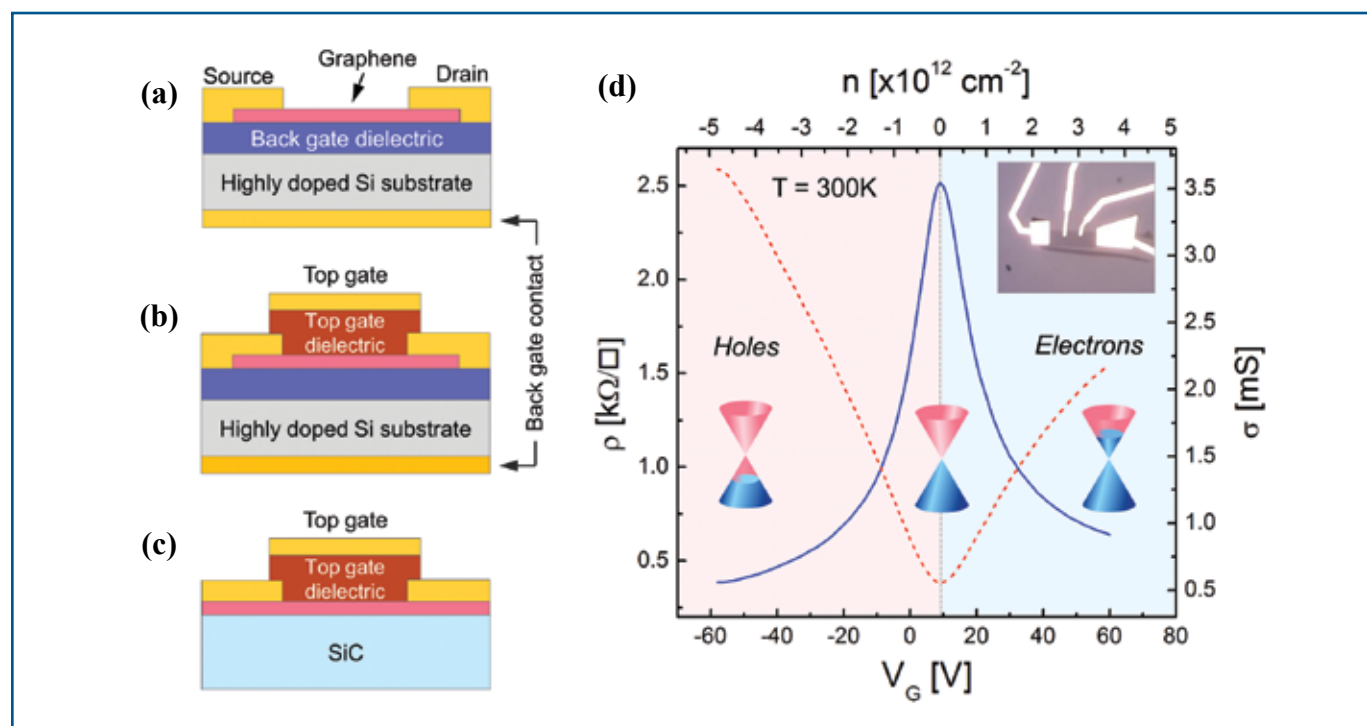


FIG. 1. (a) Back-gated graphene transistor; (b) dual-gate graphene transistor; (c) epitaxial graphene from SiC and transistor structure; (d) typical transfer curve for a single-layer graphene transistor: channel resistivity (blue line) and channel conductivity (red dashed line) vs. gate voltage. The inset in (d) shows an optical microscope image of the graphene transistor. The distance between the two outer electrodes is 10 μm .

Bilayer Graphene Transistors

gap created in such a ribbon is dependent on the C-configuration of the ribbon.²¹⁻²² Apart from lithographic patterning,²³⁻²⁴ different routes have been reported in order to make GNRs in a controlled and reproducible way (for size dimensions, not chirality) such as dispersion of graphite leading to GNRs with different widths ranging from 50 nm to sub 10 nm.²⁵ Another approach is to use Ar plasma etching to unzip multi-walled carbon nanotubes partially embedded in a poly(methyl methacrylate) (PMMA) matrix resulting in GNRs of 10-20 nm including smooth edges.²⁶ Nanowires are also used as a physical protective mask for oxygen plasma etching of graphene²⁷ resulting in nanoribbons of sub-10 nm in dimension. Considering the band gap of $E_g \sim 1.38/W$, where W is the ribbon width, I_{ON}/I_{OFF} ratios in the range of $10^2 - 10^5$ are found, while the carrier mobilities are in the order of $50-200 \text{ cm}^2 \text{ V}^{-1} \text{ s}^{-1}$. These mobility values are smaller as compared to those of conventional graphene FETs, which can be attributed to a relative increase in edge scattering events of charge carriers in the GNRs.

So far we have discussed single layer graphene (SLG) based transistors. A radically different approach can be pursued by using bilayer graphene (BLG).²⁸ BLG consists of two graphene layers, typically arranged in the Bernal (AB) stacking arrangement and interacting via their π -bonds (Fig. 2a). It is a fascinating and complex system on its own, distinct from both the monolayer graphene and the traditional two-dimensional electron gases (2DEG), even though it shares some characteristics of each. The study of bilayer graphene started in 2006 by McCann *et al.*,²⁹ who demonstrated that the low-energy band structure of neutral BLG is gapless and exhibits a variety of second-order effects. Low-energy band structure, as well as the formation of a gap when a transverse electric field is applied, have been discussed.³⁰⁻³¹

One unique feature of bilayer graphene is the ability to open a tunable energy band gap by engineering a potential difference between the two layers as is shown in Fig. 2b. Theoretical investigations predict a sizable bandgap opening up to 300 meV in AB stacking BLG using a perpendicular

electric field³²⁻³³ (Fig. 2c). The bilayer graphene is the only known material having a tunable band gap. Therefore, BLG offers possibilities of designing novel types of 2DEGs-based devices inaccessible with the use of conventional semiconductor-based 2DEGs. So far, the bandgap opening in BLG by vertical symmetry breaking has been achieved in two main flavors; either by creating a transverse electric field between the layers, *i.e.*, electrostatic gating, or by external dopants.

In the first band gap opening method the gate electrode is used for the generation of an electric displacement field. In this method, an external gate stack in direct contact with the BLG (*e.g.*, a top gate stack) is used to establish an electric displacement field perpendicular to the BLG plane. The field induces two different excess charge densities on the two layers of BLG, thus inducing a charge density asymmetry between the two layers.^{28,34} The Coulomb interaction between the two asymmetric charges causes the opening of a bandgap between the conduction and valence energy bands in the BLG band diagram. An optical bandgap of 250 meV has been measured by infrared spectroscopy³⁵ (Fig. 2c).

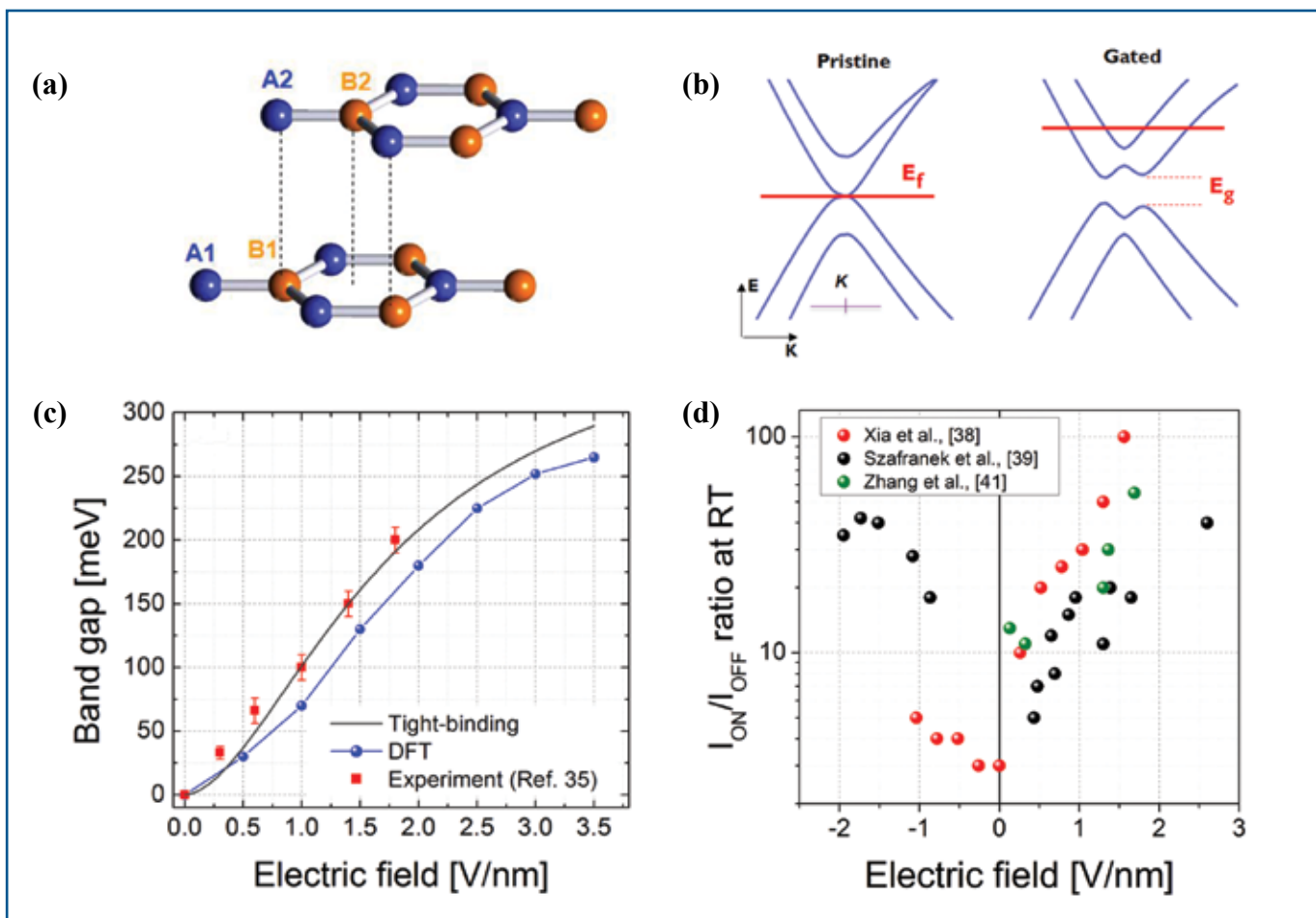


FIG. 2. (a) Schematic of the AB-stacked BLG; (b) schematic of the electronic band structure of pristine BLG (in absence of gate voltage) and gated BLG; (c) band gap dependence in BLG on the applied displacement electric field: tight-binding and DFT calculations vs. experimental data from Ref. 36; and (d) data on I_{ON}/I_{OFF} versus displacement electric field strength taken from the literature.

In order to achieve a 300 meV bandgap, the applied electric field has to be larger than 3.5 V/nm. When one applies such a high electric field across BLG, the charge density in BLG exceeds 10^{13} cm^{-2} . Therefore, to switch off the transistor, the primary gate must generate a very high electric displacement field to compensate the excess charge and bring the Fermi level into the bandgap. Another discouraging aspect of this approach is that, in order to be able to induce the required magnitude of the electric field, the top gate stack should include a dielectric with sufficiently high k , in direct contact with BLG. So far, atomic layer deposition (ALD) has been employed to deposit high- k dielectric materials (e.g., Al_2O_3) on graphene, and electric fields as high as 2.5 V/nm have been achieved.³⁵⁻³⁷ Xia *et al.*³⁸ have grown the ALD high- k on BLG after protecting the graphene surface with a polymer buffer layer. The polymer layer facilitates the ALD HfO_2 deposition through adsorption on methyl and hydroxyl groups. The combination of the polymer with HfO_2 allows for displacement electric fields only as high as 2.2 V/nm. This field corresponds to a bandgap in BLG of only 130 meV, in turn enabling a BLG-FET $I_{\text{ON}}/I_{\text{OFF}}$ of ~ 100 at room temperature.³⁸

In the second bandgap opening method, the top layer of BLG is doped by the physisorption of atoms or molecules. When considering BLG, an effective electric field can be induced by placing excess charge on the top layer, resulting in charge redistribution and asymmetry between top and bottom layers. Doping BLG by chemical physisorption resembles the effect of external gating. So far, the opening of a bandgap in BLG via physisorption has been performed by using metal adatoms deposited on top of BLG, such as potassium and aluminum,³⁹⁻⁴⁰ by evaporation of organic molecules,¹⁴ and also by doping with oxygen or even moisture.⁴¹ However, the doping approaches listed are not easily controlled and hardly compatible with a typical CMOS process flow. As it was mentioned earlier, doping of BLG only on the top side results in the formation of a high charge density in the graphene. Moreover, the electric fields achievable with the techniques listed above are insufficient to open a bandgap large enough for achieving high $I_{\text{ON}}/I_{\text{OFF}}$ ratios (Fig. 2d).

Graphene Photodetectors

Detection or sensing of light is one of the major challenges in contemporary electronics as most of the detectors are based on solid-state technology devices. The general operation principle of such photodetectors includes: (1) carrier generation by absorption of an incident photon in a semiconducting layer, (2) carrier transport and multiplication if available, and finally (3) extraction of the photo-generated carriers as a junction or device current.⁴²

The electron-hole pair generation rate is proportional to the incident photon flux and the absorption coefficient. Due to its zero band gap nature, graphene will absorb photons of all frequencies from visible to infrared range. It has been demonstrated theoretically and experimentally that single layer graphene absorbs 2.3% of incident light, a significant value for a material that is only one atom thick.⁴³⁻⁴⁴ However, excited carrier lifetimes are very short in graphene, therefore, photoexcited e-h pairs will not contribute to the device channel current. In spite of that, the graphene-metal interface was found to show increased photocurrent under the local light illumination.⁴⁵⁻⁴⁶ A close look at the conventional back-gated graphene transistor and its band diagram under different gate bias is shown in Fig. 3. Three regions can be distinguished. Region I is the metal controlled region, II is the transition region, and III is the graphene-only region. In Region I the workfunction is only defined by metal electrode; Region III is a graphene-only segment. Region II is a transition between graphene and metal: a difference between the metal workfunction

and the Fermi level of graphene $\Delta\phi$ (Fig. 3b) creates a small local electric field. This electric field can be compensated or enhanced depending on the applied V_G value and it is responsible for separation of the photogenerated e-h pairs (Fig. 3). Due to the high carrier mobility in graphene, such a detector offers enormous operation speeds (above 500 GHz, limited only by the detector's RC value) lying beyond the limits of state of the art silicon photonics devices.⁴⁷ Nevertheless, due to graphene's semimetallic nature, this kind of photodetector has rather low sensitivity, practically, not exceeding 10^{-3} A/W and limited internal quantum efficiency not exceeding 10%. By stacking a few layers one could increase light absorption in graphene.⁴⁷ Strong coupling to plasmonic oscillations was also found to enhance the photoresponse of the graphene-metal junction detector.⁴⁸

Another way to realize photodetectors with the use of graphene is to follow an approach involving band-gap opening in graphene. As mentioned above, by tailoring

(continued on next page)

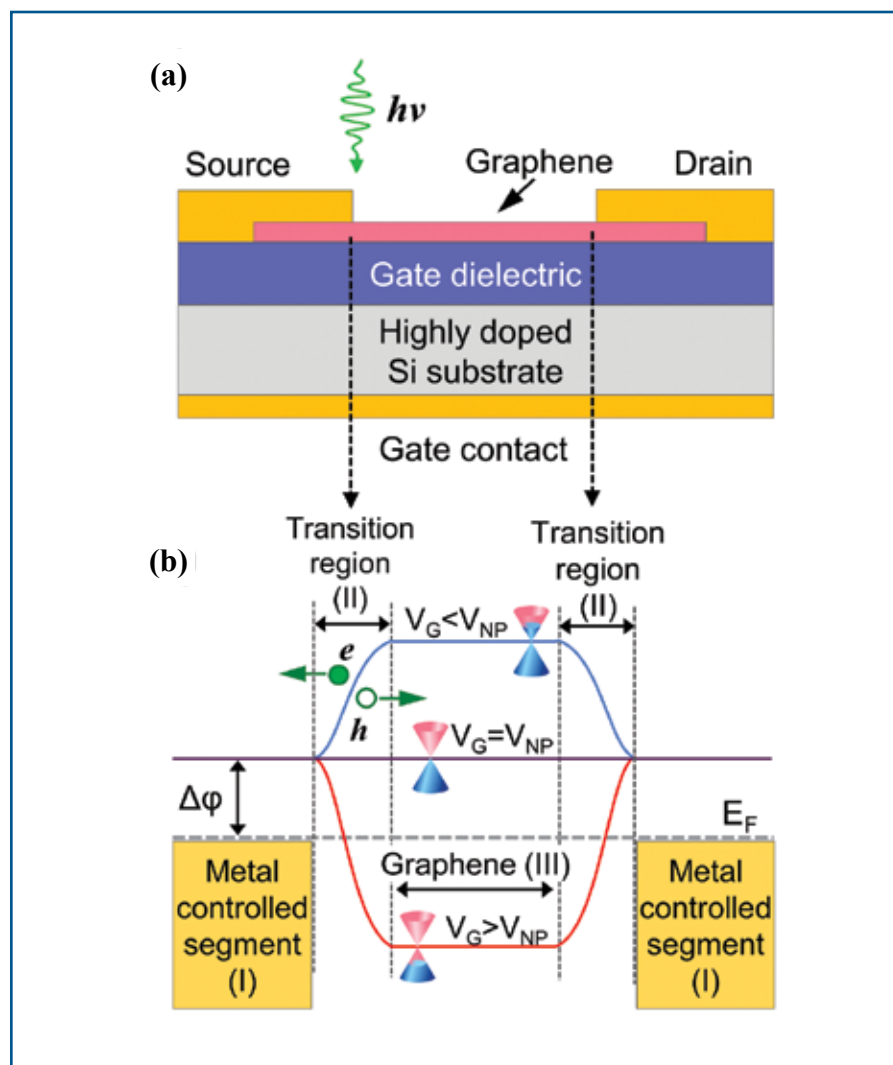


FIG. 3. Back-gated graphene transistor under light illumination (a) and its band diagram under different V_G bias showing the photodetector operation principle (b).

SLG in few nm-wide ribbons, one can induce a band gap. By transforming SLG into a semiconductor, improved photodetector sensitivity has been demonstrated.⁴⁹ An alternative approach for a band-gap absorption photodetector is using the unique property of bi-layer graphene (BLG) described previously. A BLG-based infrared bolometer based has been reported.⁵⁰ However, the majority of light-detection applications needs devices operating in the visible-light range ($\lambda = 0.4\text{--}0.8 \mu\text{m}$).

A completely different approach would be to use graphene as a carrier extractor and transfer material while bringing it in contact with a strong light absorbing material. For the latter, colloidal II-VI semiconducting quantum dots were chosen for the first time.⁵¹ The quantum dots (QDs) are chemically synthesized and they have size-dependent optical properties, which makes them attractive for biological as well as optoelectronic applications.⁵² Tuning the QD size allows one to vary the spectral response from near UV to near IR wavelengths.

The most popular II-VI quantum dots have a CdSe core covered with ZnS shell passivating the dangling bonds and acting as a wide band-gap window. Therefore, these QDs are usually referred as CdSe/ZnS.

A sub-monolayer of CdSe/ZnS QDs can be formed by spin casting over a conventional back-gated graphene device.⁵¹ The transfer characteristics I_{DS} vs. V_{G} of the pristine SLG transistor are illustrated in Fig. 4b, showing a neutrality point voltage $V_{\text{NP}} \sim 0.2 \text{ V}$, corresponding to negligible p-doping. After the deposition of QDs, the transfer characteristics shows a shift of V_{NP} from $\sim 0.2 \text{ V}$ toward negative voltages (Fig. 4b), indicating the occurrence of electron accumulation even in dark conditions inducing the charge of $n = 1.5 \times 10^{12} \text{ cm}^{-2}$. During the laser excitation ($1 \mu\text{W}$, 532 nm), a shift of V_{NP} toward more negative voltages is observed, indicating that the electron accumulation in SLG is magnified by the interaction with the charge released by the optically excited QDs. The two conduction states (corresponding to the laser ON/OFF states) can be cycled reproducibly yielding a shift in V_{NP} corresponding to a relative

increase of induced charge $\Delta n = n_{\text{laserON}} - n_{\text{laserOFF}} \sim 1.4 \times 10^{12} \text{ cm}^{-2}$. Figure 4c shows the energy level diagram for the graphene-QD system under study. The electron transfer is due to tunneling through the ZnS shell while leaving the quantum dot positively charged. The photon flux illuminating the graphene-quantum dot phototransistor can be estimated as $\Phi = 8.5 \times 10^{12} \text{ s}^{-1} \text{ cm}^{-2}$. Therefore, the external quantum efficiency, given as a ratio of induced number of electrons over the number of photons illuminating the device channel is $\text{EQE} = 1.4 \times 10^{12} / 8.5 \times 10^{12} = 16\%$. In the same time, device sensitivity can be estimated as $S = 100 \text{ nA} / 1 \mu\text{W} = 0.1 \text{ A/W}$. Both values are significantly better than those reported for conventional graphene-metal junction photodetectors. Moreover, the photon absorption occurs everywhere along the graphene surface. One could easily apply another type of photosensitizing medium, *e.g.*, other semiconducting quantum dots or organic molecules suitable for electronic interaction with graphene. A duplicate type of graphene photodetector, employing the same principle of operation and PbS quantum dots, was reported recently.⁵³

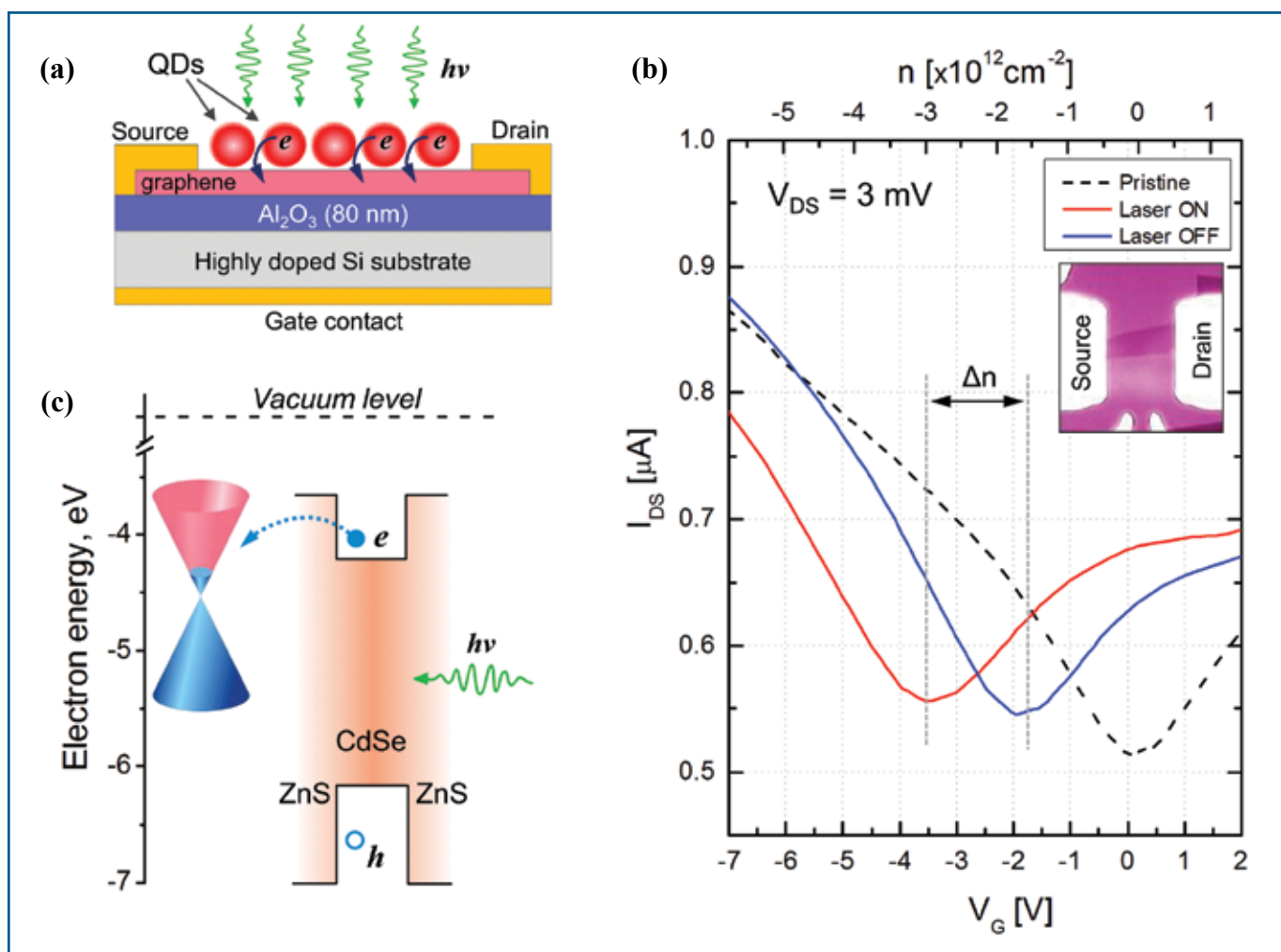


Fig. 4. (a) Back-gated graphene transistor fabricated on $\text{Si}/\text{Al}_2\text{O}_3$ sensitized with quantum dots under light illumination. (b) Transfer curves of graphene-quantum dot photodetector during its operation. (c) Schematic band diagram of graphene-QDs contact under optical excitation.

Tunable Barrier and Tunneling Effect Devices

Finally, we would like to mention another graphene-based device promising for switching. The operating principle is different from that of traditional planar MOSFET-like configurations. As mentioned before, one of the most important properties of graphene is a strong electric field effect, revealed in the electrostatically tunable Fermi level (or graphene's work function). Practically, linear energy dispersion at low density of states in graphene, for a given gate voltage change, leads to a greater change in Fermi energy as compared with classical parabolic dispersion two-dimensional electron gases. This feature offers a convenient possibility of designing structures where the key element is a tunable barrier height. Practical realization of these structures is a straightforward procedure considering the intrinsic flatness and 2D nature of graphene. The first type of devices employ quantum-mechanical tunneling effect as a key operation principle. Imagine conventional back-gated SLG-FET, but with a thin insulating layer over it and another graphene layer on top of that. Both SLG sheets are controlled by the back-gate bias, but the top layer has a different degree of gating due to the increased distance from the gate and the electrostatic screening by the bottom layer being strongly dependent on V_G . Thus, by setting constant voltage between the two SLGs, one can measure a dramatic difference in the current when sweeping the V_G . This current is due to the tunneling of either electrons or holes from one graphene layer to another.

Thanks to recent progress in developing graphene structures supported by exfoliated hexagonal boron nitride (h-BN) such a device has been demonstrated in a graphene-h-BN sandwich configuration.⁵⁴ By applying h-BN as an atomically flat insulating layer an I_{ON}/I_{OFF} ratio of up to 50 has been demonstrated and use of MoS_2 for the same purpose gave values above 10^4 . Since the tunneling process takes a negligible amount of time (at the level of femtoseconds), these devices will have enormous switching speeds going beyond that of conventional planar FETs. Another type of structure reported recently utilizes silicon-graphene Schottky junctions where the Fermi level of graphene is tuned by a local gate.⁵⁵ This structure is referred to as variable-barrier device, or "barristor" where, by tuning the graphene's Fermi level, one can dramatically suppress or enhance the thermionic current. Authors report I_{ON}/I_{OFF} ratios as high as 10^5 , fabrication of n- and p-type barristers, and complementary structures by utilizing n- and p-doped silicon layers respectively. Both types of devices described above have two important properties: (1) their speed performance does not depend directly on the

mobility of the materials involved; and (2) there's no loss of performance if the lateral size decreases below 20 nm; hence, they meet the requirements of next technology roadmap.

Summary

Single layer graphene transistors demonstrate low I_{ON}/I_{OFF} ratio at room temperature. While they show promising results when applied for high-speed analog circuits in the GHz range, their implementation for logic devices is not favorable. Opening the band gap by means of quantum confinement improves the I_{ON}/I_{OFF} dramatically, but at the cost of decrease of device channel mobility. Therefore, graphene based FET research will be concentrated around the band-gap opening in bilayer graphene by means of vertical electric fields. Although there are several challenging points in the realization of BLG-FET, it has a chance to demonstrate high enough I_{ON}/I_{OFF} ratio at a moderate carrier mobility. It is reasonable to assume that future graphene device research will also keep a strong focus on the tunneling or variable-barrier configuration structures. Graphene-metal junction based photodetectors are suitable for operation at a GHz bandwidth, but they exhibit low sensitivity and quantum efficiency. In order to enhance the latter parameters, a composite device structure, e.g., a graphene-quantum dot photodetector, would be more applicable. Further optimization of this approach would be a combination of QDs with band-gap opening in BLG. ■

About the Authors

INGE ASSELBERGHS obtained her PhD in chemistry at the KULeuven in 2003 in the field of nonlinear optics. She continued working in the group of Cor Claeys, as a post-doctoral fellow of the Foundation for Scientific Research Flanders, and in 2011 she obtained the position of researcher at IMEC, Belgium. Currently, she is affiliated with the KULeuven as a guest lecturer. Her main research topics are in field of manipulating and characterizing graphene and other 2D materials by various techniques. She may be reached at inge.asselberghs@imec.be.

STEFAN DE GENDT is a manager and principal scientist at IMEC, Belgium and full professor (part time) at the Katholieke Universiteit Leuven, Belgium. He is a Technical Editor of the *ECS Journal of Solid State Science and Technology* and *ECS Solid State Letters*. His research interests include semiconductor cleaning and surface passivation, carbon and non-carbon 2D nanomaterials, high- k dielectrics, and analytical metrology. Stefan De Gendt is a Fellow of The Electrochemical Society. He has edited books and conference

proceedings, and is the author of over 300 refereed publications. He may be reached at stefan.deGendt@imec.be.

MARC HEYNS received his PhD from the KULeuven in 1986 and joined IMEC in the same year. As Department Director and Program Director, he was responsible for exploratory research on nanotechnology, novel materials, and devices for ultimate CMOS. He became an IMEC Fellow in 2001 and a Professor at the KULeuven in 2005. His main current research interests are novel materials and devices for beyond CMOS technologies and energy storage. He has authored or co-authored more than 450 publications in scientific peer-reviewed journals, more than 900 contributions at scientific conferences (including more than 80 invited presentations), has edited or contributed to various books, and holds more than 50 patents. He has been a chair or organizer of various international scientific conferences. He may be reached on [marc.heyns@imec.be](mailto:heyns@imec.be).

ALEXANDER KLEKACHEV is performing his doctoral research at Katholieke Universiteit Leuven (KULeuven) and Interuniversity Microelectronics Centre (IMEC), Belgium. His areas of interest includes graphene electronics and optoelectronics as well as optoelectronic properties of other 2D materials and semiconducting quantum dots. He may be reached at alexander.klekachev@imec.be.

AMIRHASAN NOURBAKHSH obtained his PhD in the field of graphene electronics from KULeuven, Belgium in 2012. He is currently a FWO postdoctoral fellow at IMEC working on development of graphene for high-frequency electronics. His research interests include high performance nanoelectronics, nanofabrication and characterization, and computational physics. He may be reached at amirhasan.nourbakhsh@imec.be.

ANDRE STESMANS received his PhD in physics in 1977 and is currently serving as a full professor in the Physics Department of the Katholieke Universiteit Leuven, Belgium. His current research interests are in semiconductor physics, including interfaces of low dimensional semiconductor/insulator heterostructures, embedded semiconductor nanoparticles, high mobility semiconductors, quantum structures for photovoltaic application, point defects, and magnetic properties studied by magnetic resonance. He is a chartered physicist of the UK Institute of Physics, and local coordinator for the European Erasmus exchange program. He has contributed to various books and is (co)author of over 400 peer refereed publications. He may be reached at andre.stesmans@fys.kuleuven.be.

(continued on next page)

References

1. H. Castro Neto, F. Guinea, N. M. R. Peres, K. S. Novoselov, and A. K. Geim, *Rev. Mod. Phys.*, **81**, 109 (2009).
2. K. S. Novoselov, A. K. Geim, S. V. Morozov, D. Jiang, M. I. Katsnelson, I. V. Grigorieva, S. V. Dubonos, and A. A. Firsov, *Nature*, **438**, 197 (2005).
3. F. Chen, J. L. Xia, D. K. Ferry, and N. J. Tao, *Nano Lett.*, **9**, 2571 (2009).
4. D. B. Farmer, H. Y. Chiu, Y. M. Lin, K. A. Jenkins, F. N. Xia, and P. Avouris, *Nano Lett.*, **9**, 4474 (2009).
5. A. K. Geim and K. S. Novoselov, *Nat. Mater.*, **6**, 183 (2007).
6. R. Van Noorden, *Nature*, **469**, 14 (2011).
7. K. S. Novoselov, A. K. Geim, S. V. Morozov, D. Jiang, Y. Zhang, S. V. Dubonos, I. V. Grigorieva, and A. A. Firsov, *Science*, **306**, 666 (2004).
8. P. Blake, E. W. Hill, A. H. C. Neto, K. S. Novoselov, D. Jiang, R. Yang, T. J. Booth, and A. K. Geim, *Appl. Phys. Lett.*, **91**, 063124 (2007).
9. A. Klekachev, M. Cantoro, A. Nourbakhsh, M. H. V. d. Veen, F. Clemente, A. L. Stesmans, B. Sels, M. Heyns, and S. D. Gendt, *ECS Trans.*, **19**, 5, 201 (2009).
10. C. Berger, Z. M. Song, X. B. Li, X. S. Wu, N. Brown, C. Naud, D. Mayou, T. B. Li, J. Hass, A. N. Marchenkov, E. H. Conrad, P. N. First, and W. A. de Heer, *Science*, **312**, 1191 (2006).
11. C. Faugeras, A. Nerriere, M. Potemski, A. Mahmood, E. Dujardin, C. Berger, and W. A. de Heer, *Appl. Phys. Lett.*, **92**, 011914 (2008).
12. W. A. de Heer, C. Berger, M. Ruan, M. Sprinkle, X. Li, Y. Hu, B. Zhang, J. Hankinson, and E. Conrad, *Proceedings of the National Academy of Sciences* (2011).
13. J. H. Chen, C. Jang, S. Adam, M. S. Fuhrer, E. D. Williams, and M. Ishigami, *Nat. Phys.*, **4**, 377 (2008).
14. C. Coletti, C. Riedl, D. S. Lee, B. Krauss, L. Patthey, K. von Klitzing, J. H. Smet, and U. Starke, *Phys. Rev. B*, **81**, 235401 (2010).
15. D. B. Farmer, Y. M. Lin, A. Afzali-Ardakani, and P. Avouris, *Appl. Phys. Lett.*, **94**, 213106 (2009).
16. A. Ghosh, D. J. Late, L. S. Panchakarla, A. Govindaraj, and C. N. R. Rao, *J. Exp. Nanosci.*, **4**, 313 (2009).
17. F. Schwierz, *Nat. Nano*, **5**, 487 (2010).
18. Y. M. Lin, K. A. Jenkins, A. Valdes-Garcia, J. P. Small, D. B. Farmer, and P. Avouris, *Nano Lett.*, **9**, 422 (2009).
19. Y. Q. Wu, K. A. Jenkins, A. Valdes-Garcia, D. B. Farmer, Y. Zhu, A. A. Bol, C. Dimitrakopoulos, W. J. Zhu, F. N. Xia, P. Avouris, and Y. M. Lin, *Nano Lett.*, **12**, 3062 (2012).
20. Y.-M. Lin, A. Valdes-Garcia, S.-J. Han, D. B. Farmer, I. Meric, Y. Sun, Y. Wu, C. Dimitrakopoulos, A. Grill, P. Avouris, and K. A. Jenkins, *Science*, **332**, 1294 (2011).
21. K. Nakada, M. Fujita, G. Dresselhaus, and M. S. Dresselhaus, *Phys. Rev. B*, **54**, 17954 (1996).
22. K. Wakabayashi, M. Fujita, H. Ajiki, and M. Sigrist, *Phys. Rev. B*, **59**, 8271 (1999).
23. M. Y. Han, B. Ozyilmaz, Y. B. Zhang, and P. Kim, *Phys. Rev. Lett.*, **98**, 206805 (2007).
24. Z. Chen, Y.-M. Lin, M. J. Rooks, and P. Avouris, *Physica E: Low-dimensional Systems and Nanostructures*, **40**, 228 (2007).
25. X. L. Li, X. R. Wang, L. Zhang, S. W. Lee, and H. J. Dai, *Science*, **319**, 1229 (2008).
26. L. Y. Jiao, L. Zhang, X. R. Wang, G. Diankov, and H. J. Dai, *Nature*, **458**, 877 (2009).
27. J. Bai, X. Duan, and Y. Huang, *Nano Lett.*, **9**, 2083 (2009).
28. E. McCann, *Phys. Rev. B*, **74**, 161403 (2006).
29. K. Kechedzhi, V. I. Falko, E. McCann, and B. L. Altshuler, *Phys. Rev. Lett.*, **98**, 176806 (2007).
30. T. Ohta, A. Bostwick, T. Seyller, K. Horn, and E. Rotenberg, *Science*, **313**, 951 (2006).
31. K. S. Novoselov, E. McCann, S. V. Morozov, V. I. Fal'ko, M. I. Katsnelson, U. Zeitler, D. Jiang, F. Schedin, and A. K. Geim, *Nat. Phys.*, **2**, 177 (2006).
32. E. McCann, *Phys. Rev. B*, **74**, 161403 (2006).
33. E. V. Castro, K. S. Novoselov, S. V. Morozov, N. M. R. Peres, J. M. B. L. Dos Santos, J. Nilsson, F. Guinea, A. K. Geim, and A. H. C. Neto, *Phys. Rev. Lett.*, **99**, 216802 (2007).
34. E. McCann, *Phys. Status Solidi B*, **244**, 4112 (2007).
35. Y. B. Zhang, T. T. Tang, C. Girit, Z. Hao, M. C. Martin, A. Zettl, M. F. Crommie, Y. R. Shen, and F. Wang, *Nature*, **459**, 820 (2009).
36. T. Taychatanapat and P. Jarillo-Herrero, *Phys. Rev. Lett.*, **105**, 166601 (2010).
37. S. L. Li, H. Miyazaki, H. Hiura, C. A. Liu, and K. Tsukagoshi, *ACS Nano*, **5**, 500 (2011).
38. F. N. Xia, D. B. Farmer, Y. M. Lin, and P. Avouris, *Nano Lett.*, **10**, 715 (2010).
39. B. N. Szafranek, D. Schall, M. Otto, D. Neumaier, and H. Kurz, *Nano Lett.*, **11**, 2640 (2011).
40. E. Rotenberg, T. Ohta, A. Bostwick, T. Seyller, and K. Horn, *Science*, **313**, 951 (2006).
41. C.-T. L. Wenjing Zhang, Keng-Ku Liu, Teddy Tite, Ching-Yuan Su, Chung-Huai Chang, Yi-Hsien Lee, Chih-Wei Chu, Kung-Hwa Wei, Jer-Lai Kuo, and Lain-Jong Li, *ACS Nano*, **5**, 7517 (2011).
42. S. M. Sze, *Physics of Semiconductor Devices*, Wiley (1981).
43. R. R. Nair, P. Blake, A. N. Grigorenko, K. S. Novoselov, T. J. Booth, T. Stauber, N. M. R. Peres, and A. K. Geim, *Science*, **320**, 1308 (2008).
44. K. F. Mak, M. Y. Sfeir, Y. Wu, C. H. Lui, J. A. Misewich, and T. F. Heinz, *Phys. Rev. Lett.*, **101**, 196405 (2008).
45. T. Mueller, F. Xia, M. Freitag, J. Tsang, and P. Avouris, *Phys. Rev. B*, **79**, 245430 (2009).
46. F. N. Xia, T. Mueller, R. Golizadeh-Mojarad, M. Freitag, Y. M. Lin, J. Tsang, V. Perebeinos, and P. Avouris, *Nano Lett.*, **9**, 1039 (2009).
47. F. Xia, T. Mueller, Y.-M. Lin, A. Valdes-Garcia, and P. Avouris, *Nat. Nano*, **4**, 839 (2009).
48. T. J. Echtermeier, L. Britnell, P. K. Jasnias, A. Lombardo, R. V. Gorbachev, A. N. Grigorenko, A. K. Geim, A. C. Ferrari, and K. S. Novoselov, *Nat. Commun.*, **2**, 458 (2011).
49. B. Chitara, L. S. Panchakarla, S. B. Krupanidhi, and C. N. R. Rao, *Adv. Mater.*, **23**, 5339 (2011).
50. J. Yan, M. H. Kim, J. A. Elle, A. B. Sushkov, G. S. Jenkins, H. M. Milchberg, M. S. Fuhrer, and H. D. Drew, *Nat. Nano*, **7**, 472 (2012).
51. A. V. Klekachev, M. Cantoro, M. H. van der Veen, A. L. Stesmans, M. M. Heyns, and S. De Gendt, *Physica E*, **43**, 1046 (2011).
52. V. I. Klimov, *Nanocrystal Quantum Dots*, p. 485, CRC Press, Taylor and Francis Group, LLC (2010).
53. K. Konstantatos, M. Badioli, L. Gaudreau, J. Osmond, M. Bernechea, F. P. G. de Arquer, F. Gatti, and F. H. L. Koppens, *Nat. Nano*, **7**, 363 (2012).
54. L. Britnell, R. V. Gorbachev, R. Jalil, B. D. Belle, F. Schedin, A. Mishchenko, T. Georgiou, M. I. Katsnelson, L. Eaves, S. V. Morozov, N. M. R. Peres, J. Leist, A. K. Geim, K. S. Novoselov, and L. A. Ponomarenko, *Science*, **335**, 947 (2012).
55. H. Yang, J. Heo, S. Park, H. J. Song, D. H. Seo, K.-E. Byun, P. Kim, I. Yoo, H.-J. Chung, and K. Kim, *Science*, **336**, 1140 (2012).